CHINESE OPTICS LETTERS | Fast Track

Vol. 21, No. 6 | June 2023

On-chip ultraviolet second-harmonic generation in lithium-tantalate thin film microdisk

Miao Xue (薛 苗)[1,†], Xiongshuo Yan (颜雄硕)[1,†], Jiangwei Wu (吴江威)[1,†], Rui Ge (葛 睿)[1], Tingge Yuan (袁汀格)[1], Yuping Chen (陈玉萍)[1*], and Xianfeng Chen (陈险峰)[1,2,3]

[1] State Key Laboratory of Advanced Optical Communication Systems and Networks, School of Physics and Astronomy, Shanghai Jiao Tong University, Shanghai 200240, China

[2] Shanghai Research Center for Quantum Sciences, Shanghai 201315, China

[3] Collaborative Innovation Center of Light Manipulations and Applications, Shandong Normal University, Jinan 250358, China

*Corresponding author: ypchen@sjtu.edu.cn

Received March 18, 2023 | Accepted March 29, 2023 | Posted Online April 19, 2023

The compact and reliable ultraviolet (UV) source has attracted remarkable attention for its potential use in optical measurement systems, high-density optical storage, and biomedical applications. We demonstrate ultraviolet generation by frequency doubling in a lithium-tantalate-on-insulator (LTOI) microdisk via modal phase matching. The 50-μm-diameter microdisk was milled by a focused ion beam (FIB) and followed by chemo-mechanical polishing (CMP) to smooth the disk surface and edge, and the *Q*-factor reaches 2.74×10^5 in the visible band. On-chip UV coherent light with a wavelength of 384.3 nm was achieved, which shows great promise for using LTOIs in integrated ultraviolet source platforms.

Keywords: lithium-tantalate thin film; ultraviolet light; second-harmonic generation.
DOI: 10.3788/COL202321.061902

1. Introduction

Ultraviolet (UV) light generation devices have further advantages in many applications such as optical data storage, optical information processing, and optical sensors[1,2]. The UV region, defined as the wavelength range from 10 nm to 400 nm, is further subdivided into four distinct regions: UV-A or long-wave UV (320–400 nm); UV-B or mid-wave UV (290–320 nm); UV-C or short-wave UV (200–290 nm); and vacuum UV (10–200 nm). Second-harmonic generation both in bulk and waveguide devices via quasi-phase-matching has been studied in crystals such as $KTiOPO_4$[3–8] $LiNbO_3$, and $LiTaO_3$. However, UV light generation from quasi-phase-matching materials has several limitations, such as lower transmittance in the UV wavelength region, optical damage, and difficulties in fabrication. To solve these problems, in this work we experimentally obtained an on-chip long-wave UV in lithium-tantalate-on-insulator (LTOI) microdisk via modal phase matching frequency doubling, and the high optical *Q* of our LTOI microdisk in the visible band implies its great potential for cavity-enhanced nonlinear optics.

Lithium tantalate is a positive uniaxial crystal with ferroelectric properties, widely used in acousto-optic, electro-optic, integrated optics, nonlinear optics[9,10] and holographic data storage[11]. Recently, emerging materials in the form of thin films with unprecedented optical properties have led to revolutionary advances in integrated photonics[12]. It is worth mentioning that on-chip microresonators on the novel lithium niobate on insulator (LNOI) platform have attracted much attention[13–15]. Nonlinear processes such as second-harmonic generation (SHG)[16], sum-frequency generation (SFG)[17], parametric downconversion[18], and cascaded wave mixing[19], have been reported in LNOI microresonators, as well as single-frequency ultra-narrow linewidth on-chip microlasers[20]. Valley waveguide[21] and bichromatic cavities[22] based on lithium niobate photonic crystals have also been proposed. Compared to lithium niobate, the lithium tantalate is transparent in a larger wavelength range (0.28–5.5 μm)[23], as shown in Table 1, which can be a useful supplement in achieving UV coherent light for the lithium niobate.

At present, there are few studies on LTOI, and most of the researches are based on lithium tantalate bulk materials[28,29]. The LTOI features a higher laser-radiation-induced damage threshold[30] and a higher photorefractive damage threshold[31]. However, it is also notable that the second-order nonlinear coefficient d_{33} of the LT is smaller than that of the LN, and in the case of uniaxial crystal, the properties of d_{eff} can refer to Ref. [32].

In the following section, we give a detailed analysis of the LTOI microdisk with an optical *Q*-factor of up to 2.74×10^5, obtaining UV coherent radiation produced at the second harmonic. For efficient SHG, it is necessary to satisfy energy and

Table 1. Comparison of the Optical Parameters of Lithium Tantalate ($LiTaO_3$, LT) and Lithium Niobate ($LiNbO_3$, LN).

Crystals	$LiNbO_3$ (LN)	$LiTaO_3$ (LT)	Ref.
Transparency range at '0' transmittance level	0.40–5.5 μm	0.28–5.5 μm	[24]
Second-order nonlinear coefficient	$\|d_{33}\|$ = 41.7 pm/V	$\|d_{33}\|$ = 26 pm/V	[25,26]
Laser-induced surface damage threshold	0.005–0.03 GW/cm^2	0.22 GW/cm^2	[24]
	(at 1064 nm and 10 ns)	(at 1060 nm and 30 ns)	
Photorefractive damage threshold at 532 nm	1 kW/cm^2	2000 kW/cm^2	[27]

momentum conservations simultaneously, and the finite element method (FEM) is used to calculate the phase-matching condition. The demonstration of the on-chip realization of the ultraviolet band lithium tantalate thin film paves the foundation for using an ultraviolet source in photonic integrated circuits (PICs).

2. Device Design and Fabrication

Various methods have been used to fabricate high-Q ferroelectric domain thin film microcavities, such as femtosecond laser micromachining assisted with chemo-mechanical polishing (CMP)[33,34], electron beam lithography (EBL) combined with an inductively coupled plasma reactive ion etching (ICP-RIE) tool[35], and wet etching method[36]. UV-lithography, Ar^+ plasma etching, and HF etching techniques are also used in fabricating on-chip lithium niobate microdisk resonators[25], as well as using optimized lift-off metallic masks and dry etching processes[37]. Here, using a focused ion beam, we design and fabricate a lithium-tantalate-on-insulator microdisk in an improved method, followed by chemo-mechanical polishing. The fabrication process starts with a Z-cut LTOI chip, which has a sandwich structure (600-nm LT crystal, 2-μm silica, and 500-μm silicon substrate). The 50-μm-diameter microdisk is milled by a focused ion beam (FIB, ZEISS Auriga), as shown in Fig. 1(a). To achieve a high quality factor, a two-step milling is adopted. The parameters of the ion beam, such as current and dose, were optimized to reduce the roughness of the disk periphery. Chemo-mechanical polishing was used to smooth the disk surface and edge [Fig. 1(b)]. The sample was then immersed into a buffered oxide etching (BOE) solution, as shown in Fig. 1(c), and the silica under the LT microdisk was etched to be a pedestal. Figure 1(d) shows the morphology of the fabricated microdisk cavity.

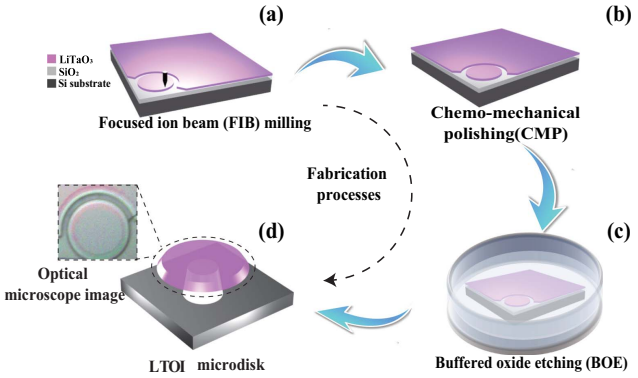

Fig. 1. Illustration of the fabrication flow. (a) Microdisk fabrication using a focused ion beam. (b) Chemo-mechanical polishing. (c) Buffered oxide etching corrodes the silica. (d) Fabricated microdisk; the inset is a zoomed-in optical microscope image.

3. Experimental Setup and Analysis

After fabricating the LTOI microdisk resonator, we conduct the optical characterization and experimental observation of an effective UV SHG process. As plotted in Fig. 2(a), the pump laser in the visible band is scanned with a speed around 0.2 nm/s and

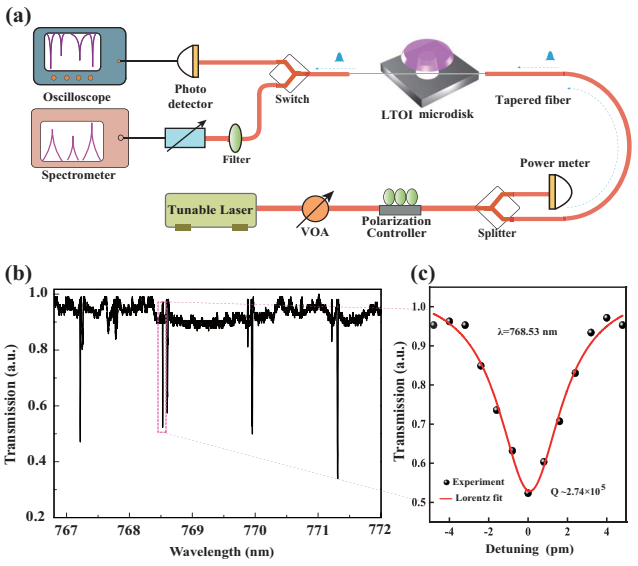

Fig. 2. LTOI experimental setup and optical characterization. (a) The experimental setup for nonlinear processes generated in the LTOI microdisk. VOA, variable optical attenuator. (b) and (c) are the transmission spectrum and Lorentzian fitting of a measured mode around 768.53 nm, respectively.

launched into the LTOI microdisk by the tapered fiber. The diameter of the 780-nm-tapered fiber is about 1–2 μm. The UV SHG signal is generated and coupled out from the microdisk with the pump light in the same tapered fiber. To separate the pump light and UV, we filter out the visible pump light by using a short-pass filter. Then, the UV signal is sent into the spectrometer for spectral analysis. The polarization and power of the pump light are controlled by the polarization controller (PC) and variable optical attenuator (VOA), respectively. We obtained the transmission spectrum of the whispering-gallery mode (WGM) in the visible band, shown in Fig. 2(b), and the central wavelength at 768.53 nm shows that the loaded optical Q-factor is 2.74×10^5, as shown in Fig. 2(c).

When increasing the optical input power, we obtained UV coherent radiation produced at the second harmonic. The ultraviolet frequency doubling signal light around 384.30 nm is generated when the optical input power is up to 17 mW and is gradually enhanced with the enhancement of the pump light. The emission spectrum around 384.30 nm is shown in Fig. 3(a). The power-dependent performance of the UV SHG on the visible input is shown in Fig. 3(b). The quadratic correlation between the pump light and UV SH signal power, well confirms that the UV signal is generated by the SHG of LTOI microdisk originating from the $\chi^{(2)}$ nonlinearity.

The UV generation in the LTOI microdisk can be described with the coupled-mode equation,

$$\begin{aligned}\frac{da}{dt} &= -\frac{\alpha_a}{2}a - i\Delta_a a + i\omega_a \kappa L a^* b + \sqrt{\eta}a_{\text{in}},\\ \frac{db}{dt} &= -\frac{\alpha_b}{2}b - i\Delta_b b + \frac{i}{2}\omega_b \kappa L a^2,\end{aligned} \tag{1}$$

where a and b are the intracavity field amplitudes of ω_a and ω_b ($\omega_b = 2\omega_a$), respectively. α_a and α_b are the respective loss rates. $\Delta_a = \varpi_a - \omega_a$ and $\Delta_b = \varpi_b - \omega_b$ are the detunings between the corresponding cavity resonance frequencies ϖ_a, ϖ_b and ω_a, ω_b, respectively. L is the cavity length; $\kappa = \frac{\sqrt{2}d_{\text{eff}}K}{cn_a\sqrt{\varepsilon_0 cn_b S}}$ is the nonlinear coupling coefficient, where d_{eff} is the nonlinear coefficient and $K = \text{sinc}(\Delta\beta L/2)$ is a dimensionless factor that relates to the phase mismatch $\Delta\beta$. n_a and n_b are the effective refractive indices of the field a, b, c is the speed of light, ε_0 is the vacuum permittivity, and S is the mode overlap area. $\eta = \theta_a/t_R$ represents the average coupling rate of the ω_a field. t_R is the roundtrip time, and θ_a is the corresponding coupling rate. Considering the undepleted-pump approximation, we can obtain the power conversion efficiency from the coupled-mode equation as

$$\xi = \frac{64\omega_a^2\kappa^2\eta^2 t_R\theta_b}{(4\Delta_a^2 + \alpha_a^2)^2[\alpha_c^2 + 4(2\Delta_a + \Delta_b^2)]}P_{\text{in}}, \tag{2}$$

where $P_{\text{in}} = |a_{\text{in}}^2|$ is the pump power. The ratio of ξ/P_{in} is related to the phase-matching condition, the propagation losses, and the mode profiles. For a fixed propagation loss, the highest efficiency can be achieved when it satisfies the perfect phase matching and critically coupled condition.

Figure 3(c) shows the effective refractive indices calculated by the finite element method of the input pump light in the visible band and the SHG signal in the UV band, which shows a phase-matched pump wavelength around 768.50 nm at a temperature of 25°C. Insets in Fig. 3(c) show the simulated mode profile of the fundamental wave (FW) and the UV second harmonic, respectively. In the Z-cut LTOI microdisk resonator, the optical axis is vertical to the device plane and the quasi-transverse-electric (quasi-TE) mode whose polarization mainly lies in the device plane as well. What is more, for three-wave mixing processes in the microdisk resonator, the discretization of the propagation constant converts the phase-matching condition into the phase mismatch $\Delta m = 0$[38]. According to the mode profiles of FW and UV second harmonic, the modal phase matching is satisfied in the LTOI microdisk. Figure 3(d) shows the observed intracavity SHG power as a function of the intracavity pump power square, and the normalized conversion efficiency is 5.74×10^{-6} W^{-1}. There are two main reasons for this inefficiency. First, only one tapered fiber is used to collect the coupled ultraviolet light, which has a low coupling efficiency. In addition, after the ultraviolet light comes out, we put it into the spatial filter and then collect it into the spectrometer, which produces a large loss. It should be noted that we use the same tapered fiber to couple the input pump light in the visible band and the UV second harmonic. To filter out the input pump light, the generated UV signal needs to pass a spatial filter before being received into the spectrometer. In fact, the generated UV signal should be

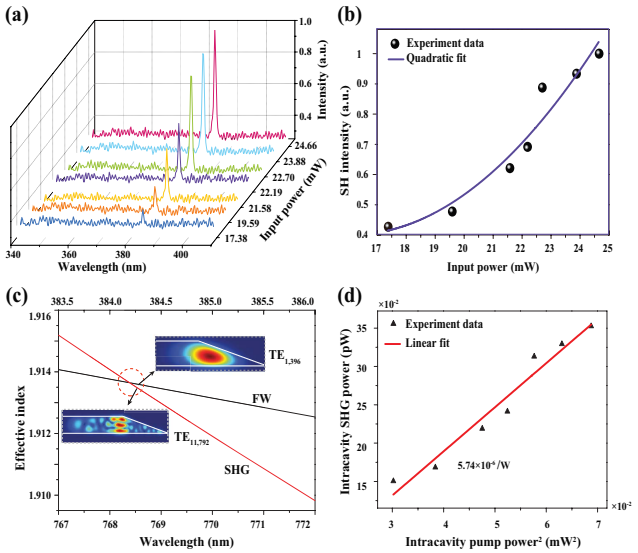

Fig. 3. Ultraviolet (UV) second-harmonic generation in the LTOI microdisk. (a) The recorded spectrum of the UV SHG signal (around 384.3 nm) is produced by the pump light in the visible band with a different power. (b) The power dependence of the UV SHG signal on the visible fundamental pump. (c) The effective indices as functions of the wavelength, of $TE_{1,396}$ in the visible band, and of $TE_{11,792}$ in the UV band, where q is the radial mode number and m is the azimuth mode number for $TE_{q,m}$. The insets show the simulated mode profiles of the FW and UV SH waves. (d) Intracavity pump power dependency of the generated SH power.

higher. To improve the conversion efficiency, one can carefully design the dispersion and domain structure carefully, and the Q-factor of the microdisk can be further improved. Also, the coupling and filtering schemes can be optimized[39].

4. Conclusion

In conclusion, we have successfully obtained an efficient 384.3 nm UV-A SHG in the efficient nonlinear material lithium tantalate, which is, to the best of our knowledge, the first to reach the on-chip UV band in an LTOI microdisk with the normalized conversion efficiency of 5.74×10^{-6} W^{-1}. Moreover, one can obtain ultraviolet light to the medium-wave UV (UV-B, 280 to 320 nm) by optimizing the pump wavelength, power, and phase-matching conditions. Higher efficiencies will be realized by further optimization of the domain structure and experimental schemes. The on-chip UV light realized by the small device size is conducive to integrating and generating a more compact UV source.

Acknowledgement

This work was supported by the National Key R&D Program of China (No. 2019YFB2203501), the National Natural Science Foundation of China (Nos. 12134009 and 91950107), Shanghai Municipal Science and Technology Major Project (2019SHZDZX01-ZX06), and SJTU (No. 21X010200828).

†These authors contributed equally to this work.

References

1. N. Savage, "Ultraviolet lasers," Nat. Photonics **1**, 83 (2007).
2. S. Tzortzakis, D. Anglos, and D. Gray, "Ultraviolet laser filaments for remote laser-induced breakdown spectroscopy (LIBS) analysis: applications in cultural heritage monitoring," Opt. Lett. **31**, 1139 (2006).
3. M. G. Roelofs, A. Suna, W. Bindloss, and J. D. Bierlein, "Characterization of optical waveguides in $KTiOPO_4$ by second harmonic spectroscopy," J. Appl. Phys. **76**, 4999 (1994).
4. K. Kintaka, M. Fujimura, T. Suhara, and H. Nishihara, "High-efficiency $LiNbO_3$ waveguide second-harmonic generation devices with ferroelectric-domain- inverted gratings fabricated by applying voltage," J. Light. Technol. **14**, 462 (1996).
5. B. Mu, X. Wu, Y. Niu, Y. Chen, X. Cai, Y. Gong, Z. Xie, X. Hu, and S. Zhu, "Locally periodically poled LNOI ridge waveguide for second harmonic generation [Invited]," Chin. Opt. Lett. **19**, 060007 (2021).
6. K. Mizuuchi, K. Yamamoto, and H. Sato, "Domain inversion in $LiTaO_3$ using proton exchange followed by heat treatment," J. Appl. Phys. **75**, 1311 (1994).
7. K. Mizuuchi and K. Yamamoto, "Harmonic blue light generation in bulk periodically poled $LiTaO_3$," Appl. Phys. Lett. **66**, 2943 (1995).
8. K. Mizuuchi and K. Yamamoto, "Generation of 340-nm light by frequency doubling of a laser diode in bulk periodically poled $LiTaO_3$," Opt. Lett. **21**, 107 (1996).
9. S. V. Tovstonog, S. Kurimura, and K. Kitamura, "High power continuous-wave green light generation by quasiphase matching in Mg stoichiometric lithium tantalate," Appl. Phys. Lett. **90**, 051115 (2007).
10. Z. D. Gao, S. N. Zhu, S.-Y. Tu, and A. H. Kung, "Monolithic red-green-blue laser light source based on cascaded wavelength conversion in periodically poled stoichiometric lithium tantalate," Appl. Phys. Lett. **89**, 181101 (2006).
11. P. Dittrich, B. Koziarska-Glinka, G. Montemezzani, P. Günter, S. Takekawa, K. Kitamura, and Y. Furukawa, "Deep-ultraviolet interband photorefraction in lithium tantalate," J. Opt. Soc. Am. B **21**, 632 (2004).
12. J. Liu, F. Bo, L. Chang, C.-H. Dong, X. Ou, B. Regan, X. Shen, Q. Song, B. Yao, W. Zhang, C.-L. Zou, and Y.-F. Xiao, "Emerging material platforms for integrated microcavity photonics," Sci. China Phys. Mech. **65**, 104201 (2022).
13. A. Boes, B. Corcoran, L. Chang, J. Bowers, and A. Mitchell, "Status and potential of lithium niobate on insulator (LNOI) for photonic integrated circuits," Laser Photonics Rev. **12**, 1700256 (2018).
14. Y. Jia, J. Wu, X. Sun, X. Yan, R. Xie, L. Wang, Y. Chen, and F. Chen, "Integrated photonics based on rare-earth ion-doped thin-film lithium niobate," Laser Photonics Rev. **16**, 2200059 (2022).
15. Y. Chen, "Photonic integration on rare earth ion-doped thin-film lithium niobate," Sci. China Phys. Mech. **65**, 294231 (2022).
16. J. Lin, Y. Xu, Z. Fang, M. Wang, N. Wang, L. Qiao, W. Fang, and Y. Cheng, "Second harmonic generation in a high-Q lithium niobate microresonator fabricated by femtosecond laser micromachining," Sci. China Phys. Mech. **58**, 1 (2015).
17. Z. Hao, L. Zhang, A. Gao, W. Mao, X. Lyu, X. Gao, F. Bo, F. Gao, G. Zhang, and J. Xu, "Periodically poled lithium niobate whispering gallery mode microcavities on a chip," Sci. China Phys. Mech. **61**, 114211 (2018).
18. R. Luo, H. Jiang, S. Rogers, H. Liang, Y. He, and Q. Lin, "On-chip second-harmonic generation and broadband parametric down-conversion in a lithium niobate microresonator," Opt. Express **25**, 24531 (2017).
19. S. Liu, Y. Zheng, Z. Fang, X. Ye, Y. Cheng, and X. Chen, "Effective four-wave mixing in the lithium niobate on insulator microdisk by cascading quadratic processes," Opt. Lett. **44**, 1456 (2019).
20. J. Lin, S. Farajollahi, Z. Fang, N. Yao, R. Gao, J. Guan, L. Deng, T. Lu, M. Wang, H. Zhang, W. Fang, L. Qiao, and Y. Cheng, "Electro-optic tuning of a single-frequency ultranarrow linewidth microdisk laser," Adv. Photonics **4**, 036001 (2022).
21. R. Ge, X. Yan, Y. Chen, and X. Chen, "Broadband and lossless lithium niobate valley photonic crystal waveguide [Invited]," Chin. Opt. Lett. **19**, 060014 (2021).
22. R. Ge, X. Yan, Z. Liang, H. Li, J. Wu, X. Liu, Y. Chen, and X. Chen, "Large quality factor enhancement based on cascaded uniform lithium niobate bichromatic photonic crystal cavities," Opt. Lett. **48**, 113 (2023).
23. J.-P. Meyn and M. M. Fejer, "Tunable ultraviolet radiation by second-harmonic generation in periodically poled lithium tantalate," Opt. Lett. **22**, 1214 (1997).
24. D. N. Nikogosyan, *Nonlinear Optical Crystals: A Complete Survey* (Springer Science & Business Media, 2005).
25. J. Wang, F. Bo, S. Wan, W. Li, F. Gao, J. Li, G. Zhang, and J. Xu, "High-Q lithium niobate microdisk resonators on a chip for efficient electro-optic modulation," Opt. Express **23**, 23072 (2015).
26. S. Matsumoto, E. J. Lim, H. M. Hertz, and M. M. Fejer, "Quasiphase-matched second harmonic generation of blue light in electrically periodically poled lithium tantalate waveguides," Electron. Lett. **27**, 2040 (1991).
27. K. Kitamura, Y. Furukawa, S. Takekawa, T. Hatanaka, H. Ito, and V. Gopalan, "Non-stoichiometric control of $LiNbO_3$ and $LiTaO_3$ in ferroelectric domain engineering for optical devices," Ferroelectrics **257**, 235 (2001).
28. A. A. Savchenkov, A. B. Matsko, V. S. Ilchenko, D. Seidel, and L. Maleki, "Surface acoustic wave opto-mechanical oscillator and frequency comb generator," Opt. Lett. **36**, 3338 (2011).
29. W. Xie, X. Chen, L. He, Y. Chen, and Y. Xia, "Theoretical study of quasi-phase-matching fourth harmonic generation in periodically poled lithium tantalate," Chin. Opt. Lett. **2**, 664 (2004).
30. X. Yan, Y. Liu, L. Ge, B. Zhu, J. Wu, Y. Chen, and X. Chen, "High optical damage threshold on-chip lithium tantalate microdisk resonator," Opt. Lett. **45**, 4100 (2020).
31. J. Imbrock, S. Wevering, K. Buse, and E. Krätzig, "Nonvolatile holographic storage in photorefractive lithium tantalate crystals with laser pulses," J. Opt. Soc. Am. B **16**, 1392 (1999).
32. D. A. Roberts, "Simplified characterization of uniaxial and biaxial nonlinear optical crystals: a plea for standardization of nomenclature and conventions," IEEE J. Quantum Electron. **28**, 2057 (1992).
33. R. Wu, J. Zhang, N. Yao, W. Fang, L. Qiao, Z. Chai, J. Lin, and Y. Cheng, "Lithium niobate micro-disk resonators of quality factors above 10^7," Opt. Lett. **43**, 4116 (2018).

34. J. Zhang, Z. Fang, J. Lin, J. Zhou, M. Wang, R. Wu, R. Gao, and Y. Cheng, "Fabrication of crystalline microresonators of high quality factors with a controllable wedge angle on lithium niobate on insulator," Nanomaterials **9**, 1218 (2019).
35. M. Zhang, C. Wang, R. Cheng, A. Shams-Ansari, and M. Lončar, "Monolithic ultra-high-*Q* lithium niobate microring resonator," Optica **4**, 1536 (2017).
36. R. Zhuang, J. He, Y. Qi, and Y. Li, "High-*Q* thin-film lithium niobate microrings fabricated with wet etching," Adv. Mater. **35**, 2208113 (2023).
37. K. Zhang, Z. Chen, H. Feng, W.-H. Wong, E. Y.-B. Pun, and C. Wang, "High-*Q* lithium niobate microring resonators using lift-off metallic masks [Invited]," Chin. Opt. Lett. **19**, 060010 (2021).
38. I. Breunig, "Three-wave mixing in whispering gallery resonators," Laser Photonics Rev. **10**, 569 (2016).
39. Y. Dong, K. Wang, and X. Jin, "Package of a dual-tapered-fiber coupled microsphere resonator with high *Q* factor," Opt. Commun. **350**, 230 (2015).